

Comparisons of experimental and theoretical nucleus-nucleus potentials for heavy-ion reactions

B. Sikora

Institute of Nuclear Physics, Warsaw University, Hoza 69, Warsaw, Poland

M. Blann

E-Division, Lawrence Livermore Laboratory, Livermore, California 94550

W. Scobel

I. Institut für Experimental Physik, University of Hamburg, Hamburg, West Germany

J. Bisplinghoff

Institut für Strahlen und Kernphysik, Bonn University, Bonn, West Germany

M. Beckerman

Laboratory for Nuclear Science, Massachusetts Institute of Technology, Cambridge, Massachusetts 02139

(Received 7 May 1979)

A broad range of heavy-ion-induced fusion excitation functions are classically analyzed. The fusion-barrier parameters are compared with predictions of the proximity potential, a Yukawa-plus-exponential model, and a modified Woods-Saxon potential. The Yukawa-plus-exponential model is found to give the best overall agreement with the data. The proximity potential is too shallow, but would be in closer agreement with data if a necking contribution were added.

[NUCLEAR REACTIONS Extracted fusion barriers and radii from fusion data with heavy ions, compared several theoretical models.]

I. INTRODUCTION

In this work we report on comparisons between internuclear potentials extracted from experimental heavy-ion fusion excitation function analyses and predictions of several theoretical models. These consist of proximity,¹ Yukawa plus exponential (YE),² and modified renormalized Woods-Saxon potentials (MWS).³ We have made comparisons of our data with nuclear models in the past; however, the quality and quantity of the data have now significantly improved and several new suggestions have been made as to the theoretical form of the nucleus-nucleus potential.¹⁻³

We will first review the classical method used to analyze the data and the assumptions and uncertainties which are present in such an analysis, as well as in modifications in data analysis suggested by other groups. We will then give a brief description of the three nuclear models to be considered, and investigate how well they agree with the trends of experimentally deduced results.

II. CLASSICAL ANALYSIS OF FUSION EXCITATION FUNCTION DATA

Fusion excitation functions have often been analyzed using the classical relationship⁴⁻⁷

$$\sigma_{\text{fus}}(\epsilon) = \pi R_{\text{fus}}^2 (1 - V_{\text{fus}}/\epsilon). \quad (1)$$

This expression assumes that there is an effective barrier height V_{fus} which exists at some distance between centers R_{fus} , and that the system is conservative.

Whether or not there is an effective fusion barrier depends in part on the dynamics of the coalescence process. It must be remembered that the only true multidimensional saddle point is the fission barrier. The latter is generally for a symmetric system. The target and projectile usually have neither the same mass asymmetry nor deformation of the true saddle point.

The nuclear part V_n of V_{fus} is extracted assuming that $V_{\text{fus}}(R_{\text{fus}}) = V_n(R_{\text{fus}}) + V_c(R_{\text{fus}})$, the Coulomb potential being given by point charges at separation R_{fus} .

An additional possible limitation on the use of Eq. (1), which has been pointed out, is that the position of V_{fus} has a radial centrifugal dependence in such a model, so that the average fusion radius decreases with increasing average angular momentum and therefore with bombarding energy.

Certainly some experimental excitation functions do not give the linear relationship predicted by Eq. (1) when plotted vs $1/\epsilon$ and should not be analyzed via Eq. (1). Linearity is a necessary, but not necessarily sufficient, condition in extracting R_{fus} and V_{fus} from Eq. (1).

One aspect of the uncertainty in extracting values

of V_n and R_{fus} from linear analysis of data is illustrated in Fig. 1 for the case of $^{35}\text{Cl} + ^{141}\text{Pr}$. These data, we note, are among the poorest in the entire set analyzed. In Fig. 1 we have drawn the best fitting line, giving $R_{fus} = 10.7$ fm and $V_n(10.7) = 14$ MeV. We have drawn a somewhat higher line, representing the steepest line which we feel could reasonably be drawn through the data [$R_{fus} = 11.2$ fm, $V_n(11.2) = 7.8$ MeV]. Similarly, we have drawn the line of least slope consistent with the data (10.3 fm, 19.7 MeV). In this context there appears to be a rather large uncertainty in R_{fus} and V_{fus} . However, as was pointed out by Birkelund and Huizenga,^{9,9} the correlated values of $V(R)$ versus R show the trend with R which is expected of the nucleus-nucleus potential. So while the precise value of R_{fus} may have a large uncertainty, the variation of V_n with R deduced from such analysis is subject to far less uncertainty.

The question of a nonconservative system existing in the entrance channel has been raised for the particular case of "frictional" dissipation.^{9,9} However, this should be velocity dependent,¹⁰ and one might again expect some deviation from linearity in a σ vs $1/\epsilon$ plot if such dissipation were important. It may well be that there is an important contribution to V_{fus} owing to neck formation. If this is a constant for a given system (independent of ϵ) it would be included in the result extracted from Eq. (1) but is not explicitly included in the several theoretical models to be considered. We

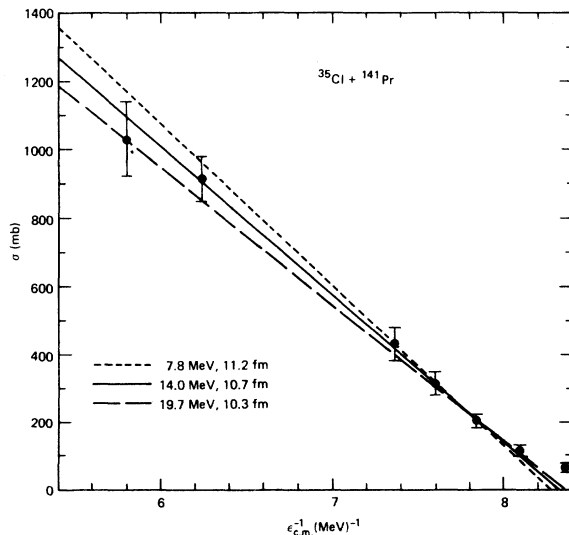


FIG. 1. Fusion cross sections versus $\epsilon_{c.m.}^{-1}$ for $^{35}\text{Cl} + ^{141}\text{Pr}$. Points with error bars are experimental results. Three possible lines are drawn through the data, and identified as to R_{fus} and $V_n(R_{fus})$ corresponding to each line, cf. Sec. II.

suspect that the very linear behavior of the $1/\epsilon$ plots over a very broad energy range for the systems we have considered supports the use of Eq. (1). But this is only an assumption at present, given no good reason to suspect the contrary. A recent theoretical treatment of fusion analysis of data of this type concludes a primary sensitivity to the conservative fusion potential and relative insensitivity to assumed dissipative forces.¹¹

An alternative method of data analysis which has been suggested consists of a least squares fit to the fusion excitation function using the formula due to Wong.¹² In these analyses, relatively low energy data are generally included since Wong's model includes effects due to barrier penetration. However, our experience has been that $V_{fus}(R_{fus})$ and R_{fus} results extracted from such analyses vary markedly depending upon the number and quality of the low energy points included in the analyses.¹² With our best data, an analysis according to Ref. 12 gives results in agreement with those from a linear analysis using Eq. (1).¹³ With these reservations in mind of the possible errors in the analyses, we consider models for the internuclear potential.

III. THEORETICAL MODELS

A. Proximity potential

The proximity potential¹ predicts the internuclear potential as being due to the separation between two semi-infinite slabs of nuclear matter, modified by a geometric curvature correction. The nuclear potential is given by

$$V_n = 4\pi\gamma\bar{R}b\Phi(\rho), \quad (2)$$

where

$$\bar{R} = \frac{C_1 C_2}{C_1 + C_2}, \quad (3)$$

with C_i being the central radii of the target and projectile. The central radius is related to the effective sharp radius by

$$C \approx R[1 - (b/R)^2], \quad (4)$$

where b is the surface thickness taken to be 1.00 fm. The parameter $\rho = s/b$, where

$$s = r - C_1 - C_2, \quad (5)$$

is the difference between the internuclear separation r and the sum of the sharp radii. The parameter γ is the liquid drop surface energy coefficient given by

$$\gamma = 0.9517\{1 - 1.7826[(N - Z)/A]^2\} \text{ MeV/fm}^2. \quad (6)$$

The effective sharp radius is defined by

$$R = 1.28A^{1/3} - 0.76 + 0.8A^{-1/3}. \quad (7)$$

The proximity function $\Phi(\rho) \simeq \Phi(S)$ is tabulated¹ in the reference; a simple analytic expression is also given. We have used the tabulated results with interpolation.

B. Yukawa-plus-exponential potential

Nix and co-workers have recently modified their earlier Yukawa potential¹⁴ to satisfy the liquid drop saturation condition at saturation density. In so doing they gained an additional range parameter.

Their prescription for the nucleus-nucleus potential may be written as

$$V_n = V_{\text{red}}(2 + S/a) \exp(-S/a), \quad (8)$$

where

$$S = r - (R_1 + R_2) \quad (9)$$

is the separation between the equivalent sharp surfaces (whereas the central radii are used to define S in the proximity model).

As an approximation, one may write

$$V_{\text{red}} = [C_s(1)C_s(2)]^{1/2} \frac{aR_1R_2}{r_0^2(R_1 + R_2)} \quad (10)$$

(valid when $R_1/a, R_2/a \gg 1$) with $C_s(i) = A_s \{1 - K_s [(N - Z)/A]^2\}$.

There are four parameters in this model, evaluated as follows: $r_0 = 1.18$ fm based on Myers's droplet model analyses of electron and muonic atom scattering; $a = 0.65$ fm, the range of the folding functions evaluated from heavy-ion elastic scattering potentials; surface energy coefficients $a_s = 21.7$ MeV, and $K_s = 3.0$ (surface-asymmetry constant) which were selected in order to reproduce fission barriers of nuclei in the rare-earth to actinide region. We note that the calculations presented in this work used the more rigorous expression of Ref. 2 for V_{red} , rather than Eq. (10).

One should note that both the proximity potential and the YE potentials have a pre-exponential dependence of the form surface energy $\times N_1N_2$, and a related exponentially decreasing range dependence; however, there is some difference as to the manner in which the relevant separation is defined. We will use the pre-exponential function in later comparisons to partially reduce all systems to a dependence on a range parameter S .

C. Modified Woods-Saxon potential

Wilczynska and Wilczyński³ have proposed a modified Woods-Saxon potential wherein the depth V_0 and range parameter a are determined from boundary conditions using the liquid drop model:

$$V_n = -V_0 [1 + \exp(r - C_1 - C_2)/a]^{-1}, \quad (12)$$

where

$$V_0 = b_{\text{surf}} [A_1^{2/3} + A_2^{2/3} - (A_1 + A_2)^{2/3}] \quad (13)$$

and

$$a = \frac{(C_1 + C_2)V_0}{C_1C_216\pi\gamma} = \frac{V_0}{16\pi\gamma R}. \quad (14)$$

The surface energy coefficient is evaluated as 17 MeV, and r, C, \bar{R} , and γ are given by Eqs. (3)–(6).

IV. COMPARISONS OF EXPERIMENTAL AND MODEL INTERNUCLEAR POTENTIALS

Comparisons of the nuclear part of the three nucleus-nucleus potentials under discussion are shown in Figs. 2 and 3 for the systems $^{35}\text{Cl} + ^{27}\text{Al}$ and $^{35}\text{Cl} + ^{141}\text{Pr}$. For the first system, the three models give quite similar values of the potential with separation S ; slopes of the proximity and Yukawa-plus-exponential functions (YE) are similar, whereas the modified Woods-Saxon (MWS) has a lesser slope with increasing radial separation. The difference in slope is also apparent for the $^{35}\text{Cl} + ^{141}\text{Pr}$ system, for which the difference in absolute magnitude of the MWS potential and the other two is much more pronounced. The MWS gives a considerably deeper nuclear potential at large separations than the proximity or Yukawa plus exponential models.

We have also indicated the positions of the maxima in the nuclear-plus-Coulomb potentials for the three models in question in Figs. 2 and 3; these distances are the fusion radii predicted by the models and $V_n(R)$, the *a priori* predicted values

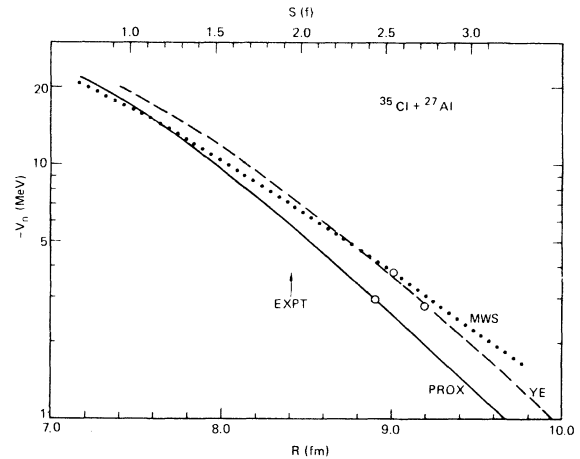


FIG. 2. Calculated nuclear potentials on three models versus separation of $^{35}\text{Cl} + ^{27}\text{Al}$. Open circles represent the *a priori* fusion barriers (V_n) predicted by each model. The arrow indicates the R_{fus} deduced from experimental results assuming the validity of Eq. (1).

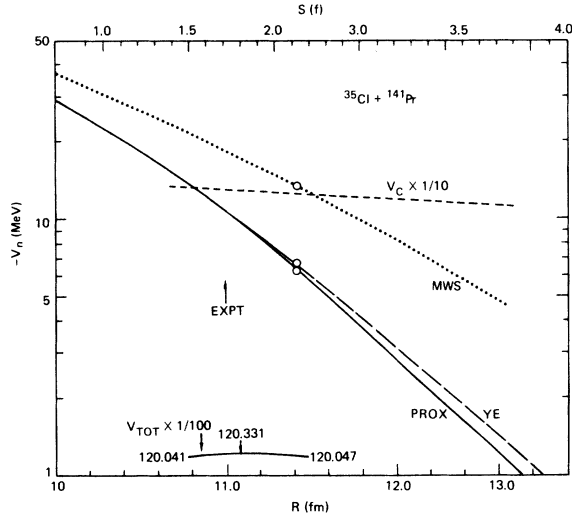


FIG. 3. As in Fig. 2 for the system $^{35}\text{Cl} + ^{141}\text{Pr}$. The Coulomb barrier has been indicated in this figure, as well as a portion of the total (Coulomb plus nuclear) potential using the proximity potential.

of the nuclear fusion-barrier potential. In Fig. 3 we have also shown the Coulomb barrier, and the sum of Coulomb plus nuclear potentials for the proximity potential. We point out that this total potential is 120.041 MeV at 10.8 fm, increases to 120.331 MeV at 11.1 fm, and then decreases to 120.047 MeV at 11.5 fm. One can ask how seriously to take the theoretically predicted position of the fusion barrier. In this example we note that a depression of the nuclear contribution of the order of 400 keV at 11.5 fm or greater, going smoothly to zero depression at 10.8 fm (due, e.g., to deformation or neck formation) or any similar relative shift in the nuclear or Coulomb potentials, could cause a 0.7 fm shift in the position predicted for the fusion barrier. This in turn would give, in this example, a 9-MeV difference in $V_n(R)$. Because small uncertainties in the slope of V_n or in V_c can cause such a catastrophic shift in the predicted radial position of the maximum of $V_n + V_c$, it may be imprudent to attempt an extraction of R_{fus} from these models. Rather, we feel that analyses of experimental data of the type discussed in the previous section, or other approaches for extracting R_{fus} from experimental excitation functions, is to be preferred. If the radius is satisfactorily extracted by such an analysis, and the nuclear potential includes, e.g., a 400-keV distortion energy, then the discrepancy to be expected *vis à vis* an otherwise correct one-dimensional model is only the 0.4 MeV. Otherwise stated, we feel that comparisons of deduced V_n at deduced R values with model predictions are reasonable com-

TABLE I. Summary of experimentally deduced and theoretical fusion-barrier radii and heights.^a

Reaction	$R_{\text{fus}}(f)$ Expt.	$V(R_{\text{fus}})$ MeV Expt.	Ref.	$V_n(R_{\text{fus}})$		$V_n(R_{\text{fus}})$		$R_{\text{fus}}(f)$		$V_n(R)$		$R_{\text{fus}}(f)$		$V_n(R)$		\bar{R}	
				proximity	YE	MWS	Expt.	proximity	proximity	proximity	YE	YE	MWS	MWS	S	S	
$^{32}\text{S} + ^{24}\text{Mg}$	8.5	27.8	4	-3.5	-4.6	-5.1	-4.6	8.7	-2.6	-2.6	8.95	-2.6	8.7	-3.2	2.33	1.536	
$^{32}\text{S} + ^{27}\text{Al}$	8.3	29.2	4	-5.2	-7.3	-6.5	-6.8	8.8	-2.7	-2.7	9.1	-2.7	8.9	-3.5	1.99	1.58	
$^{32}\text{S} + ^{40}\text{Ca}$	9.0	43.2	4	-4.9	-6.4	-6.8	-7.9	9.2	-3.8	-3.8	9.3	-4.3	9.3	-5.2	2.11	1.606	
$^{35}\text{Cl} + ^{27}\text{Al}$	8.4	30.7	6	-5.9	-7.4	-6.9	-7.1	8.9	-2.9	-2.9	9.2	-2.8	9.0	-3.8	1.98	1.712	
$^{35}\text{Cl} + ^{64}\text{Ni}$	9.7	60.3	6	-6.9	-8.2	-11.1	-10.2	9.9	-5.3	-5.3	10.05	-5.3	10.2	-7.3	1.96	1.905	
$^{35}\text{Cl} + ^{55}\text{Ni}$	9.5	60.8	6, b	-8.3	-9.3	-12.1	-10.9	9.9	-5.0	-5.0	9.9	-5.7	10.1	-7.0	1.83	1.895	
$^{35}\text{Cl} + ^{55}\text{Ni}$	9.25	61.7	6, b	-9.6	-11.3	-13.5	-12.3	9.7	-2.9	-2.9	9.8	-5.7	9.9	-7.5	1.68	1.873	
$^{40}\text{Ca} + ^{58}\text{Ni}$	9.6	72.7	c	-8.2	-9.5	-12.8	-11.0	9.8	-6.4	-6.4	9.9	-6.7	10.0	-9.0	1.84	1.93	
$^{40}\text{Ca} + ^{62}\text{Ni}$	9.0	71.3	c	-8.0	-9.8	-13.4	-11.8	9.9	-6.3	-6.3	10.0	-6.7	10.2	-8.8	1.82	1.953	
$^{35}\text{Cl} + ^{90}\text{Zr}$	9.7	83.7	6	-16.8	-16.3	-20.8	-17.3	10.4	-3.5	-3.5	10.4	-7.45	10.6	-10.0	1.35	2.016	
$^{58}\text{Ni} + ^{62}\text{Ni}$	9.3	98.6	d	-25.2	-26.7	-33.0	-22	10.3	-8.4	-8.4	10.4	-8.35	10.7	-11.5	0.84	2.114	
$^{35}\text{Cl} + ^{116}\text{Sn}$	10.2	103.7	6, 7, b	-16.4	-17.1	-23.5	-16.2	10.8	-7.8	-7.8	10.75	-8.8	11.0	-12.4	1.33	2.096	
$^{35}\text{Cl} + ^{141}\text{Pr}$	10.7	120.5	7, b	-10.6	-10.7	-18.6	-14.0	11.1	-4.8	-4.8	11.1	-9.6	11.4	-13.9	1.72	2.155	

^a Data from Refs. 4-7.

^b B. Sikora, W. Scobel, M. Beckerman, and M. Blann (unpublished).

^c B. Sikora, J. Bisplinghoff, W. Scobel, M. Beckerman, and M. Blann (unpublished).

^d B. Sikora, M. Blann, and M. Beckerman (unpublished).

parisons to make. But because very small uncertainties in V_n (or V_c) can cause very large changes in predicted radial positions of $V_n + V_c$ maxima in a one-dimensional formulation, one should not rely on such one-dimensional models for estimating R_{fus} .

Values of V_n extracted from our data using Eq. (1) and the related separations R_{fus} are summarized in Table I, where values of V_n from the three models under consideration are also tabulated at the same radii. These values are compared graphically on a plot of V_n/\bar{R} [see Eq. (3)] versus the separation between the sharp radii S [Eq. (5)] in Fig. 4. On this graph a smooth curve may be drawn through the $V_n(R)$ values of the proximity and YE potentials. Values of $V_n(R)$ predicted by the MWS potential are shown as open points; experimentally deduced results are shown as closed points with a somewhat arbitrary vertical error bar. Additionally, two sets of points have dashed lines connecting the extreme R and $V(R)$ values from the possible set of $1/\epsilon$ lines which could be drawn in Fig. 1 and the related figure for $Cl + Al$. These dashed error bars indicate (as has been pointed out previously (Sec. II) that a large part of the uncertainty in extracting V_n and R from the data is compensated in the final analysis; values at $V_n(R)$ versus R are reproduced even though there is an uncertainty in R , due to the correlation between these variables.

The trend of the data would seem to indicate that the proximity potential is too shallow at separations greater than 1.2 fm in S , increasing too rapidly with increasing S . A simple shift in S would not correct this discrepancy, as too deep a potential would be predicted at smaller S in order to get better agreement at larger S . This conclusion is similar to that reached earlier⁶ for the potential of Ngo *et al.*¹⁵ which gives results similar to the proximity potential.

That the proximity potential tends to give too little nuclear attraction at larger separations was shown in earlier comparisons with potential values deduced from both elastic scattering and fusion data.^{8,9} This may have been a part of the motivation for the YE approach, which gives a significantly better agreement (than the proximity potential) with the experimental trend and results, and which has an additional parameter available in its formulation. We should point out, however, that addition of necking effects in the proximity potential would move it closer to experimental results.

The nuclear potential values due to the MWS potential are generally deeper than experimental results at smaller values of S , giving close agreement for $S \geq 1.6$. The discrepancy is in the cor-

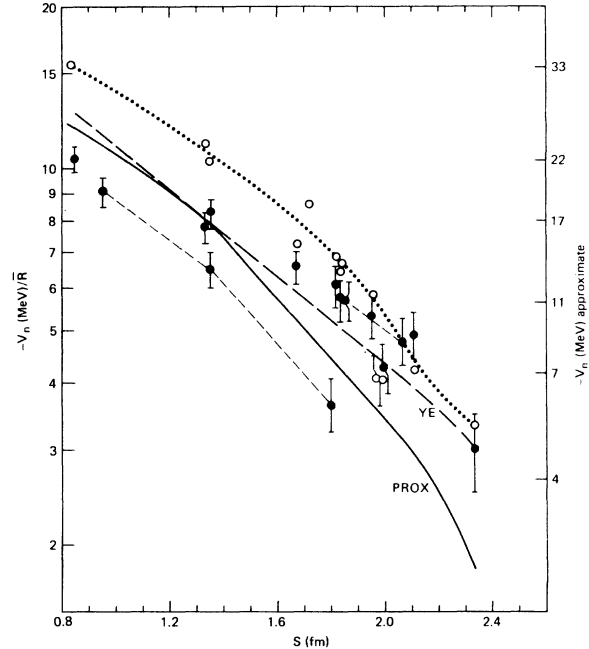


FIG. 4. Comparison of calculated and experimentally deduced nucleus-nucleus potentials V_n . The left-hand-side ordinate is the calculated or measured V_n divided by \bar{R} defined by Eq. (3). The right-hand-side ordinate gives the V_n in an approximate MeV scale. The abscissa is the separation of the sharp surfaces S as defined by Eq. (5). The proximity potential is given by the solid line; the Yukawa-plus-exponential potential, by the dashed line. The modified Woods-Saxon results are shown as open circles for the systems measured experimentally. A dotted curve shows the general trend of the MWS model. Experimentally deduced $V_n(R)$ values are shown as closed points with arbitrary \pm MeV error bars, for the systems summarized in Table I. For two points, the range of $V_n(R)$ is shown for the full range of values which could be extracted from using Eq. (1) with the data points as in Fig. 1.

rect direction if there should be a significant energy dissipation in the entrance channel, which increases with penetration. Then the experimentally deduced V_n results should be less deep than the theoretical results, the discrepancy increasing with decreasing S , and this is true for the MWS potential. The question of the significance and degree of energy dissipation at distances up to the fusion radius (or more appropriately pseudobarrier) is unfortunately an open question. We can, therefore, conclude that the proximity potential is too shallow at larger S , that the YE potential seems to give the most satisfactory agreement with all the data, and that the MWS potential may yet prove to be superior to the other two if non-conservative effects become important for $S \leq 1.6$ fm.

This work was performed under the auspices of the U. S. Department of Energy by the Lawrence

Livermore Laboratory under Contract No. W-7405-ENG-48.

-
- ¹J. Blocki, J. Randrup, W. J. Swiatecki, and C. F. Tsang, *Ann. Phys. (N.Y.)* 105, 427 (1977).
²H. J. Krappe, J. R. Nix, and A. J. Sierk, *Phys. Rev. Lett.* 42, 215 (1979).
³K. Sivek-Wilczynska and J. Wilczynski, *Phys. Lett.* 74B, 313 (1978).
⁴H. H. Gutbrod, W. G. Winn, and M. Blann, *Nucl. Phys.* A213, 267 (1973).
⁵W. Scobel, H. H. Gutbrod, M. Blann, and A. Mignerey, *Phys. Rev. C* 14, 1701 (1975).
⁶W. Scobel, H. H. Gutbrod, M. Blann, and A. Mignerey, *Phys. Rev. C* 14, 1808 (1976).
⁷P. David, J. Bisplinghoff, M. Blann, T. Mayer-Kuckuk, and A. Mignerey, *Nucl. Phys.* A287, 179 (1977).
⁸J. R. Birkelund and J. R. Huizenga, *Phys. Rev. C* 17, 126 (1978).
⁹J. R. Birkelund, J. R. Huizenga, J. N. De, and D. Sperber, *Phys. Rev. Lett.* 17, 1123 (1978).
¹⁰J. Randrup, *NORDITA Report No. 77/36*, 1977 (unpublished); W. J. Swiatecki, private communication, 1978.
¹¹U. Mosel, *Phys. Rev. C* 19, 2167 (1979).
¹²C. Y. Wong, *Phys. Rev. Lett.* 31, 766 (1973).
¹³B. Sikora, J. Bisplinghoff, W. Scobel, M. Beckerman, and M. Blann (unpublished).
¹⁴H. J. Krappe and J. R. Nix, in *Proceedings of the Third International Atomic Energy Symposium on the Physics and Chemistry of Fission*, Rochester, 1973 (IAEA, Vienna, 1974), Vol. 1, p. 159.
¹⁵C. Ngo *et al*, *Nucl. Phys.* A252, 237 (1975).